

LDA analysis of PVC-central recirculation zone interaction in a model vortex burner

C.E. Cala, E.C. Fernandes, M.V. Heitor, S.I. Shtork[†]

Laboratory of Thermofluids, Combustion and Energy Systems

Center for Innovation, Technology and Policy Research, IN+

Instituto Superior Técnico, Av. Rovisco Pais, 1049-001 Lisbon, Portugal

<http://in3.dem.ist.utl.pt>

[†] Permanent address: Institute of Thermophysics SB RAS, 630090 Novosibirsk, Russia

ABSTRACT

An LDA technique and phase averaging analysis were used to study an unsteady flow in a model vortex burner (Fig. 1a). The flow instability originated from a precessing vortex core (PVC) associated with swirling jet breakdown. In Fig. 1a, and based on phase averaged flow analysis for one time instant, the centre locations of the three vortex structures found are schematically represented: the PVC, helical central recirculation vortex (HCRV) and helical outer vortex (HOV). Eduction of the vortex structures was based on λ_2 -plots (Jeong and Hussain, 1995) similar to that shown in Fig. 1b. The map displays the outer vortex arm responsible for controlling fluid entrainment in the outer shear layer of the jet. The inner spiral arm represents the central recirculation zone (CRZ) with a non-classical structure (the CRZ is usually axisymmetric due to time averaging of data). Based on data analysis we conclude that the PVC interacts with the helical central recirculation zone, acting as a stirrer inside it, rapidly losing energy during the interaction.

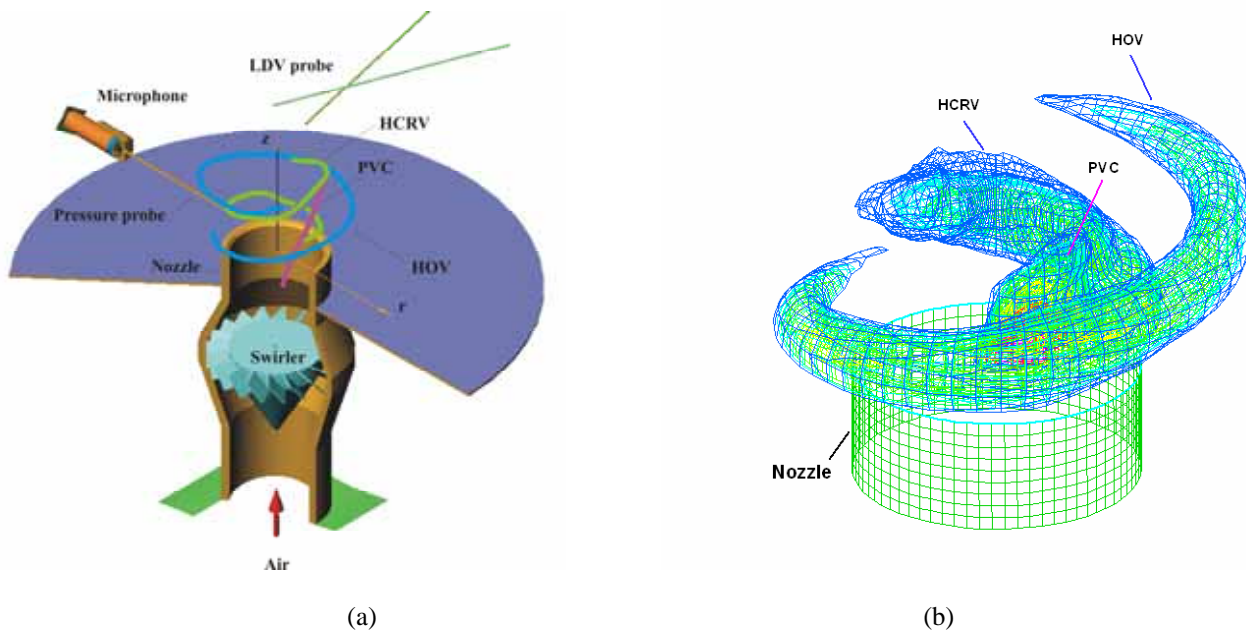


Fig. 1. (a) – Setup. (b) - Isosurfaces of dimensionless λ_2 showing large-scale coherent vortex structures associated with the PVC (plot with high threshold of $-10T_0^{-2}$; $T_0 = d/U_0$ - characteristic time, d and U_0 - nozzle diameter and mean velocity, respectively).

1. INTRODUCTION

It was shown by previous experiments (Anacleto et al., 2003) that an LPP combustion chamber operating in a swirl stabilized mode can provide ultra low NO_x emissions. This performance can only be obtained in a narrow working window (swirl v.s. equivalence ratio) while being intrinsically associated with a periodic flow pulsation, but decoupled from the acoustics of the combustor cavity. This natural flow pulsation is due to the presence of a precessing vortex core (PVC) that arises because of the specific LPP geometry (sudden expansion) and swirling flow conditions, resembling those of Chanaud (1965), Cassidy & Falvey (1970), Syred et al. (1994), Froud et al. (1995), Griffiths et al. (1998), Roehle and Willert (2001), and Selle et al. (2004).

The precessing vortex core is not fully discussed in the literature in the context of LPP technology and the natural question that arises is how the PVC interacts with the central recirculation zone, affecting the flame stability/structure and pollutant emission. In this context a study will be conducted on a geometrically simplified LPP combustor model, running isothermal flow.

2. EXPERIMENTAL TECHNIQUE

Fig. 1a shows the model burner, consisting basically of a swirler device followed by a nozzle (diameter $d = 56$ mm), ending in a sudden natural expansion. Atmospheric air loaded from a blower passes through a plenum chamber, stabilizing the air flow rate, and a straight pipe with about 20 diameters of length to obtain a nearly developed pipe flow before the test section. The air flow rate was measured at a calibrated orifice connected to a U-type water manometer. The tested case is defined here by $Re_d=15000$, $S=1$ (based on the swirler geometry) and velocity measurements were made along the radial direction for different horizontal planes.

A standard one-component Dantec LDA system operating in a forward scattering mode was employed for velocity measurements (Fernandes, 1998). Velocity data was recorded simultaneously with microphone signals to perform phase average measurements (Fernandes, 1998). The system includes a 2W Ar-Ion laser (green light with $\lambda=514.5$ nm) and a rotating grate providing frequency shifting. The optical head 310mm focal distance lens forms a measuring volume with a $44 \times 44 \times 606$ μm in size. The microphone used to generate the reference signal is a B&K-4189. The flow seeding was carried out by a single jet atomizer filled with paraffin oil and connected to a compressed air line.

The total number of LDV data points for each measured location was $N=16384 \times 3$ (three time series) covering approximately $N_{\text{cycle}}=600 \times 3$ precession cycles. Using the reference signal an averaged variation history of the velocity components during the pulsation cycle was obtained for each measured point. Whenever necessary the phase-averaged velocity data are mapped in a circular $r-\theta$ region (the signal phase angle was transformed to the angular coordinate) assuming a constant phase speed of vortex core rotation (e.g. Griffiths et al. 1998). This reconstruction for different horizontal planes results in a mean instantaneous velocity distribution in a cylindrical region. The vortical structures were identified using vorticity/ λ_2 values computed from the volume velocity data.

3. RESULTS AND DISCUSSION

To support the model of three large-scale structures plotted in Fig. 1 and to show how vortices interact detailed measurements are presented in the following paragraphs, after a description of traditional time-mean flowfield results to outline the presence of the PVC.

3.1. Time averaged flow characteristics.

The precession frequency, defined as dominant peaks in the spectra of velocity and pressure signals, is a linear function of the flow rate, with the coefficient depending on the swirling intensity. The data plotted in dimensionless form demonstrate independence of Re above 10,000 for both swirl numbers studied (Fig. 2). The case of $Re=15,181$ and $S=1.01$ (typical of the practical LPP combustor of Anacleto et al., 2003) with a precession frequency of 75.5Hz was kept throughout this work as a reference condition for detailed velocity measurements.

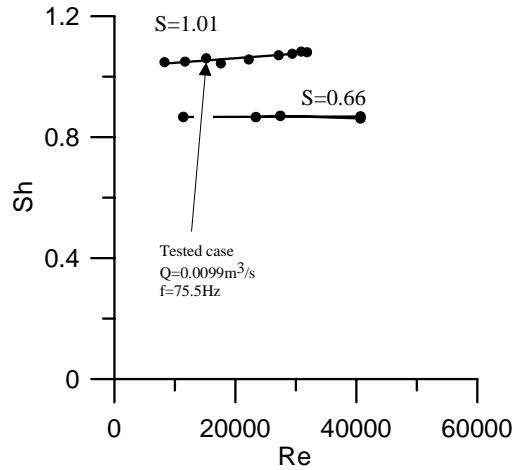


Fig. 2. Influence of Re number (flow rate) and swirl number (blade angle) on the dimensionless precession frequency (Strouhal number).

The time averaged flow structure for the tested case is shown in Fig. 3a (right plot) as stream lines calculated by integration of the radial profiles of axial velocities. Sample profiles of velocity components in two horizontal cross-sections are presented in Fig. 3b (right plot). The Figures show typical features of a strongly swirling jet with a central reverse flow (e.g. Heitor and Moreira, 1992). Maximal negative axial velocities occur at a distance of about $0.53d$ at the corresponding maximal extent in a radial direction. The ratio of maxima of tangential to axial velocities is about unity, corresponding to the swirl number value $S=1.01$ (this ratio is of an estimator for the swirl number as suggested by Gupta et al. (1984) and Gallaire and Chomaz (2003)). Close to the nozzle exit the radial velocity is relatively high and positive (pointing inwards) and is negative outside the jet, due to the air flow ejected from the ambient space. At axial distances larger than $0.53d$ the radial velocity is low and shows inward flow in the inner part of the jet and outward flow at far radii. Tangential velocity indicates absence of rotation inside the recirculation zone at the nozzle exit. Further experiments have shown that this effect suggests the presence of a strong coherent structure inducing an asymmetrical instantaneous velocity distribution, resulting in the above-mentioned time averaged flow pattern. At far cross-sections (where the PVC disappears) the inner part of the jet is filled by a solid body rotation, as expected for a forced vortex (Gupta et al., 1984).

The spatial distribution of turbulent kinetic energy and sample radial profiles of fluctuating velocity components are presented in Figs. 3a, 3b (left plots). The high level of turbulence, with a peak of 200% close to the nozzle edge, is mostly related to coherent motion in a form of a precessing vortex, as also discussed by Gupta et al. (1984). The radial distribution of tangential velocity RMS shows abnormal peaks at locations where the mean velocity exhibits minimal shear ($r=0$ and $r/d=0.45$). Sample velocity spectra taken at these points exhibit discrete frequencies, confirming a strong periodicity of the flow pulsations. At the far cross section, where the PVC disappears, the Reynolds stress distributions become more smooth and isotropic.

3.2. Phase averaged velocity field.

In Figure 4a the phase averaged flow structure induced by the PVC is presented for $z/d=0.179$ as a radial-tangential velocity vector map superimposed over a contour map of axial velocity. The precessing vortex displaced from the nozzle's geometrical centre can be clearly identified. The reverse flow zone is attached to the core centre and trailing in the vortex wake. In fact, the vortex core moves at the boundary of zero axial velocity, dividing the reverse flow zone and a local region of high forward axial velocity. The local peak of tangential velocity coincides with the positive peak of the axial component.

A 3-D spatial boundary of the instantaneous reverse zone is shown in Figure 5. The reverse zone area is clearly shifted from the centre in the lower part of the flow area ($z/d=0-0.6$) and takes a symmetrical position at distances greater than $z/d=0.7$ (see also Fig. 4b obtained for $z/d=0.714$ and showing a near axisymmetric flow pattern). A large radius spiral arm outlines a reverse flow induced by one of the secondary vortices, namely, the outer entrainment vortex (denoted as HOV in Fig. 1).

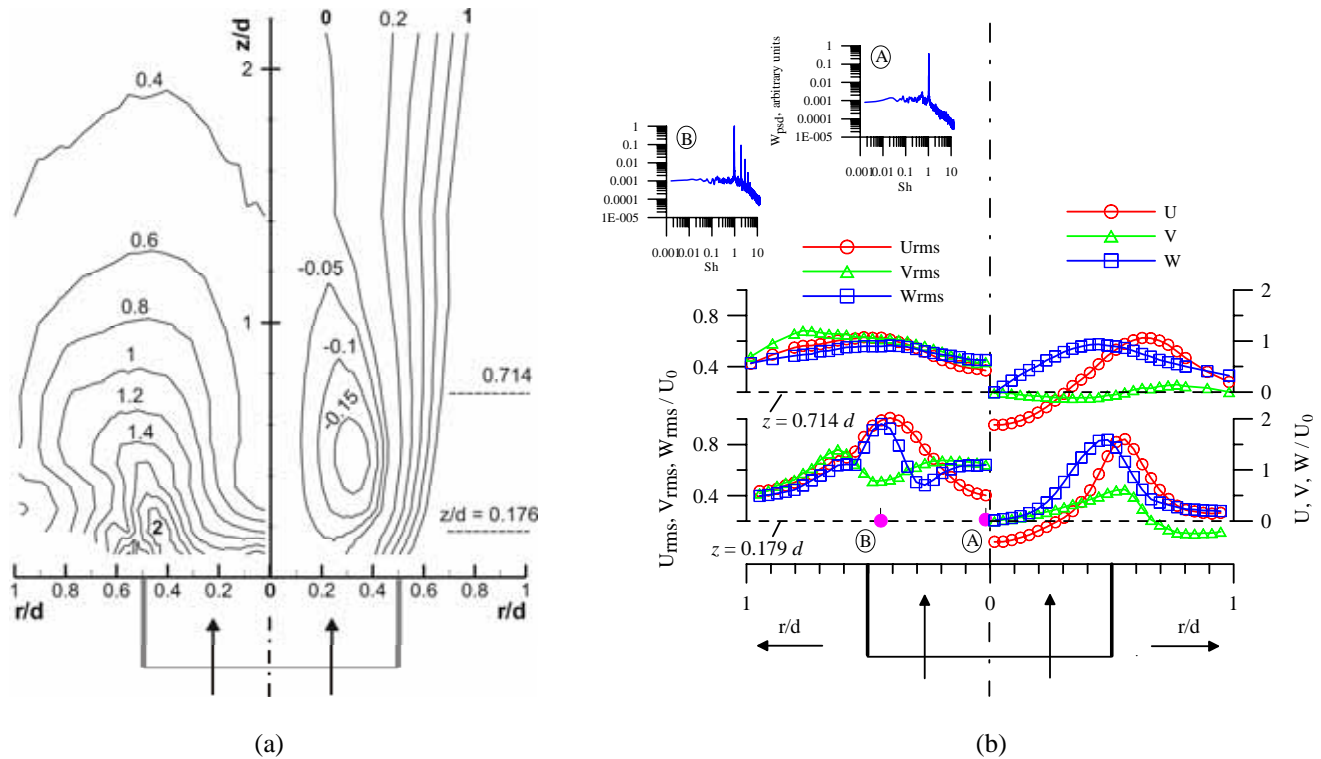


Fig. 3. Averaged flow structure for the tested case $S=1.01$, $Re=14900$:

a) - right: normalised stream function; left: normalised turbulent kinetic energy.

b) – sample profiles taken at $z/d=0.179$ and 0.714 (right - averaged velocity components, left - fluctuating velocity components). U , V , W – axial, radial, and tangential velocity components, respectively.

An important characteristic of a swirl stabilized burner system relates to the intensity of the central recirculating flow, which can be quantified as a recirculating flowrate (Fig. 6). Conventional characterization based on time averaged axial velocity profiles shows that the most intense reverse motion takes place at the distance $z/d=0.446$, which is in agreement with other authors (Heitor and Moreira, 1992; Gupta et al., 1984). However, as already noted, the phase averaged flow pattern demonstrates that in a cross-section where a strong precessing structure exists the reverse velocity absolute minimum is shifted away from the centre line. Consequently, integration over the reverse flow region gives noticeably stronger recirculating flow with the most intense reverse flow located closer to the nozzle exit ($z/d=0.268$), as presented in Fig. 6. This suggests also that a swirling flow with a precessing structure might be more effective in terms of a flame stabilization process compared to a steady axisymmetric flow without a PVC. A favourable effect of PVC on combustion performance has been reported, for example, for low calorific gas burners (Froud et al., 1995).

3.3. Vortex structures identification.

The velocity data plots shown in Fig. 4 provide expressive information on the vortical flow structure and may enable identification of the vortex core locations, although velocity based criteria do not fulfill Galilean invariance and therefore fail when applied to detect nonstationary vortices (Schram and Riethmuller, 2001). An alternative widely used criterion to deduce coherent vortex structures uses vorticity distribution. A high vorticity magnitude is an indicator of the localised vortical motion. Being based on velocity derivatives, this method enables elimination of vortex core convective velocity. This is an important feature to study travelling vortex structures as in the present case.

On the other hand, the high vorticity areas may not necessarily point to vortical structures and can be attributed to intense shear. A necessary and sufficient criterion for vortical structure identification was suggested by Jeong and Hussain, 1995, who developed the vortex definition based on the pressure minimum but eliminating unsteady straining and viscous effects. The proposed technique (the so-called λ_2 -technique) refers to the second eigenvalue λ_2 of the symmetric tensor $S^2 + \Omega^2$, where S and Ω are the symmetric and antisymmetric parts of the velocity gradient tensor ∇V (V –velocity vector). A connected region with negative λ_2 corresponds to a vortex core area. Note that this technique, being based on velocity derivatives, provides Galilean invariance.

Figure 7 presents a comparison of the PVC area maps plotted using absolute vorticity $|\omega|$ (ω - vorticity vector) and λ_2 values. Both techniques indicate the main vortex core which has the form of an ellipse, but a spot of strong vorticity near the PVC is seen, apparently due to shear motion, and is not related to a vortical motion, as can be seen by examining the λ_2 map. This example also demonstrates that Jeong and Hussain's technique allows the vortex core boundary to be depicted (as zero λ_2 values), while vorticity maps additionally require definition of a threshold level which may be subjected to a shear/background vorticity often present in the flow. Note also that the velocity vector maps indicate a vortex centre location that does not coincide with that given by the vorticity/ λ_2 extremum location which is assumed to be the vortex core centre. This discrepancy can be eliminated by an appropriate choice of the vortex convective velocity to be subtracted from the flowfield.

Absolute vorticity/ λ_2 maps do not identify vortical structure signs, which were defined here using maps of normalized helicity $H_n = (\mathbf{V} \cdot \boldsymbol{\omega}) / (|\mathbf{V}| \cdot |\boldsymbol{\omega}|)$ (Levy et al., 1990). Helicity is a scalar quantity and its graphical representation is relatively simple compared to a velocity/vorticity vector field (basically, the sense of rotation in a vortex core can be identified by analyzing the velocity and vorticity vector spatial orientations). Due to its definition the values of H_n may vary between +1 and -1 (corresponding cases of co-directed and counter-directed velocity and vorticity vectors) and its sign indicates the sense of swirl of the vortex relative to the streamwise velocity.

3.4. Secondary vortical structures.

A global flow structure is shown in Figure 8 using λ_2 for the zero high threshold level (iso-surfaces of positive levels are not plotted). The map displays the outer vortex arm (HOV) responsible for controlling fluid entrainment in the outer shear layer of the swirling jet. The inner spiral arm (HCRV) represents the central recirculation zone with a non-classical structure (as used, the CRZ is symmetrical due to time averaging of data, see Fig. 3a).

Since, the presented map does not show the main PVC, which is embedded in the central helical recirculation zone, horizontal and vertical slices of the λ_2 volume data, together with the on-plane velocity projections (radial-tangential and radial-axial components respectively), are shown in Fig. 9. The horizontal cross-axis view (Fig. 9b) allows clear recognition of the PVC hidden in the previous figure, while the vertical cross-axis view (Fig. 9a) permits identification of the non-symmetric central recirculation zone and the outer vortex structure close to the location of the main PVC.

λ_2 absolute magnitude, which in fact is related to vortex intensity (a more intense vortical structure produces lower pressure), demonstrates that the PVC is a primary vortex structure, which is assumed to control the global flow dynamics as the most powerful structure (the PVC core contains primary vorticity generated by the swirler). The inner and outer vortices can be considered as secondary vortex structures. The PVC rapidly loses intensity and vanishes at $z/d=0.6-0.7$. By contrast, the outer vortex structure keeps coherence up to $z/d=1.3-1.5$.

Figure 10 presents the helicity map in vertical cross-section (the same plane as in Fig. 9a) which cuts the secondary vortices almost perpendicularly, and it can be seen that areas of internal and external vortex structures appear with different helicity signs, indicating that these vortices are counter rotating coherent structures. The vertical cross-section also visualizes the PVC cutting it almost longitudinally (through axis). The sign combination confirms that the sense of the PVC and internal secondary vortex (HCRV) coincides with the base flow rotation and is opposite to the sense of the external vortex (HOV).

In Figure 11a a reconstruction of all vortex axes (lines connecting minima points in λ_2 maps) is re-plotted together with the corresponding rotation senses verified by the helicity maps. The axis configurations shown indicate that all the helical structures are wound opposite to the base flow rotation. This is a key feature regarding HCRV and PVC which must conjugate with a central reverse flow (those vortices whose sense of winding is consistent with the base flow rotation induce

forward velocity along the flow axis, as argued by Alekseenko et al., 1999). Interaction between the central recirculating eddy and the PVC (they are of the same sign as noted above) eventually leads to their merging with a preceding partial breakup. Note that the HCRV originates at the reverse zone base and it seems begins attaching to the PVC. Interaction and merging between the PVC and the inner recirculating eddy seems to distort the PVC core boundary into an ellipse (Meunier and Leweke, 2001) and causes rapid dissipation of the PVC.

Thus, quantitative flow visualization enabled eduction of the combination of three large-scale vortical structures presented in the studied combustor model. Although the most powerful vortex referred to here as the PVC controls the overall flow structure, the secondary vortices, HOV and HCRV, are assumed to play a significant role in combustor performance as they are the mechanism through which the swirling jet mixes with the surrounding fluid. The breakdown zone, normally associated with a single precessing spiral vortex core (Chanaud 1965), is in fact the conjunction of a pair of co-rotating co-winding spiral vortices. The PVC counterpart, referred to as the HCRV, formed by a dramatic collision between the central reverse flow and the PVC, is a minor structure under current conditions, but this disproportion may change to what has been observed as a double helical structure with equally distributed energies of the vortices (Ruith et al., 2003).

4. CONCLUSIONS

An unsteady swirling jet flow in a vortex burner has been studied using LDA and microphone techniques with phase averaging data processing. The unsteadiness was related to a precessing vortex core (PVC). Detailed measurements were made for $Re=15,000$ and $S=1.01$. The conditions correspond to a typical velocity of 4m/s and precession frequency of 75.5 Hz. The Strouhal number was found to be independent of Re . Coherent vortex structures in the gathered data were educted based on the λ_2 -technique of Joeng and Hussain (1995).

Despite the three-dimensionality of the flow structure, a classical approach based on velocity time averaging demonstrates flow patterns with an axisymmetric central recirculation zone typical of swirl stabilized burners (e.g. Heitor and Moreira, 1992) but with abnormal turbulence kinetic levels, for example 200% close to the burner exit due to the abovementioned PVC coherent motion.

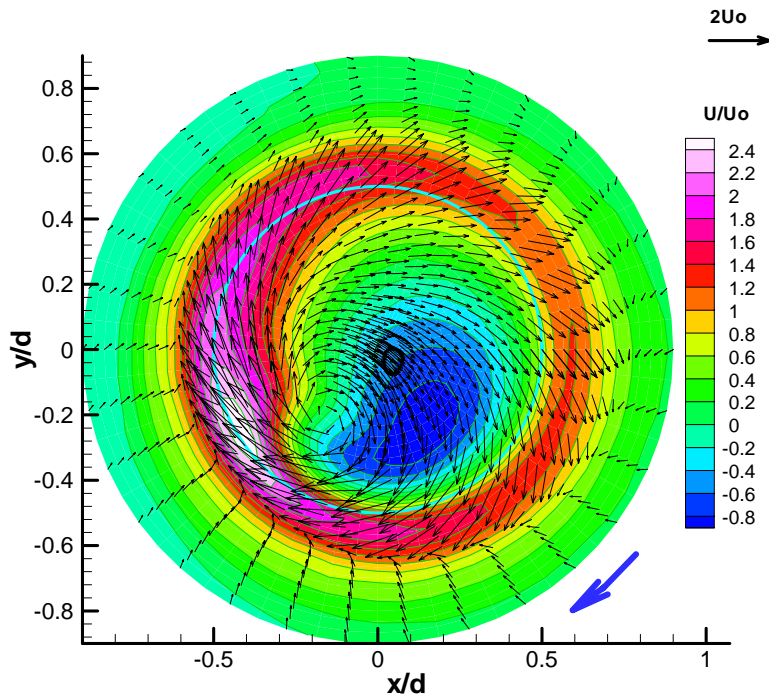
Based on analysis of phase averaged data, three main spiral vortex structures (precessing vortex core - PVC, helical central recirculation vortex - HCRV, and helical outer vortex - HOV) controlling the flow field near the burner mouth were identified. The jet breakdown zone is the conjunction of a pair of co-rotating co-winding spiral vortices (PVC and HCRV). The outer vortex (HOV) is responsible for controlling fluid entrainment in the outer shear layer of the jet. The HOV sign is opposite to the sign of the internal vortices (PVC and HCRV). All the structures are left handed spirals (sense of winding opposite to basic flow rotation) but with drastically different pitches: the PVC has a large pitch and axis aligned along the axial coordinate; the HCRV and HOV are tightly coiled helices with a small pitch and axis aligned azimuthally (orthogonally to the PVC axis). The PVC is the primary and most powerful structure (the PVC core includes primary vorticity generated by the swirler); the HCRV and HOV are considered here as secondary vortical structures. Interaction between the PVC and HCRV leads to their eventual merging and disintegration. In the near field region ($z < 0.5d$), the instantaneous central reverse flow area is intrinsically asymmetrical, following the PVC locus shifted away from the burner geometrical centre. At greater distances (after PVC dissipation) the flow becomes nearly axisymmetric.

ACKNOWLEDGEMENTS

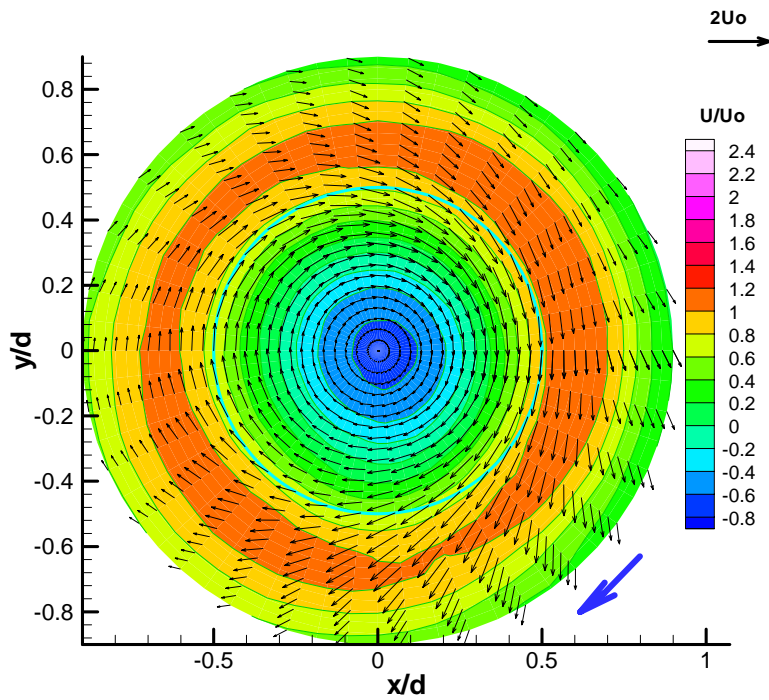
The authors are pleased to acknowledge support from the Portuguese Science and Technology Foundation (through Research Grant PCTI/1999/EME/34768 and Research Fellowship SFRH/BPD/1641/2000 provided for S.I. Shtork). The help of Mr. Eduardo Bimba in assembling the experimental setup is also gratefully appreciated.

REFERENCES

- Alekseenko, S.V., Kuibin, P.A., Okulov, V.L., and Shtork, S.I. (1999). "Helical vortices in swirl flow", *J. Fluid Mech.*, 382, pp. 195-243.
- Anacleto, P.M., Fernandes, E.C., Heitor, M.V., and Shtork, S.I. (2003). "Swirl flow structure and flame characteristics in a model lean premixed combustor", *Combust. Sci. and Tech.*, 175 (8), pp. 1369 - 1388.
- Cassidy, J.J., Falvey, H.T. (1970). "Observation of unsteady flow arising after vortex breakdown", *J. Fluid Mech.*, 41, pp. 727-736.
- Chanaud, R.C. (1965). "Observations of oscillatory motion in certain swirling flows", *J. Fluid Mech.*, 21, pp. 111-127.
- Fernandes, E.C. (1998). "The onset of combustion-driven acoustic oscillations", PhD thesis, Instituto Superior Técnico, Lisbon, Portugal.
- Froud, D., O'Doherty, T., Syred, N. (1995). "Phase averaging of the precessing vortex core in a swirl burner under piloted and premixed combustion conditions", *Comb. and Flame*, 100, pp. 407-412.
- Heitor, M.V., Moreira, A.L.N. (1992). "Velocity characteristics of a swirling recirculating flow", *Experimental Thermal and Fluid Science*, 5, pp. 369-380.
- Jeong, J., Hussain, F. (1995). "On the identification of a vortex", *J Fluid Mech.*, 285, pp. 69-94.
- Gallaire, F., Chomaz, J.-M. (2003). "Mode selection in swirling jet experiments: a linear stability analysis", *J. Fluid Mech.*, 494, pp. 223-253.
- Griffiths, A.J., Yazdabadi P.A., Syred, N. (1998). "Alternate eddy shedding set up by the nonaxisymmetric recirculation zone at the exhaust of a cyclone dust separator", *Journal of Fluids Engineering – Transactions of the ASME*, 120(1), pp. 193-199.
- Gupta, A.K., Lilley, D.G., Syred, N. (1984). "Swirl Flows", Abacus Press, Tunbridge Wells, UK.
- Levy, Y, Degani, D., and Seginer, A. (1990). "Graphical Visualization of Vortical Flows by Means of Helicity", *AIAA* 28(8), pp. 1347-1352.
- Meunier, P., Leweke, T. (2001). "Three-dimensional instability during vortex merging", *Physics of Fluids*, 13(10), pp. 2747-2750.
- Roehle, I., Willert, C.E., (2001). "Extension of Doppler global velocimetry to periodic flows", *Meas. Sci. Tech.*, 12, pp. 420-431.
- Ruith, M.R., Chen, P., Meiburg, E., Maxworthy, T. (2003). "Three-dimensional vortex breakdown in swirling jets and wakes: direct numerical simulation". *J Fluid Mech.*, 486, pp. 331-378.
- Schram, C., Riethmuller, M.L. (2001). "Vortex ring evolution in an impulsively started jet using digital particle image velocimetry and continuous wavelet analysis", *Meas. Sci. Tech.*, 12, pp. 1413-1421.
- Selle, L., Lartigue, G., Poinot, T., Koch, R., Schildmacher, K.-U., Krebs, W., Prade, B., Kaufmann, P., and Veynante, D. (2004). "Compressible large eddy simulation of turbulent combustion in complex geometry on unstructured meshes", *Comb. and Flame*, 137, pp. 489-505.
- Syred, N., O'Doherty, T., Froud, D. (1994). "The interaction of the precessing vortex core and reverse flow zone in the exhaust of a swirl burner", *Proc. of the Institution of Mechanical Engineering, Part A- J. of Power and Energy*, 208(A1), pp. 27-36.



(a)



(b)

Fig. 4. Phase-averaged velocity maps. Vectors represent the radial-tangential component while the color map shows axial velocity. a - cross-section $z/d=0.179$; b - 0.714 . The cyan circle indicates the nozzle edge. The displayed flowfields rotate clockwise as shown by the blue arrows.

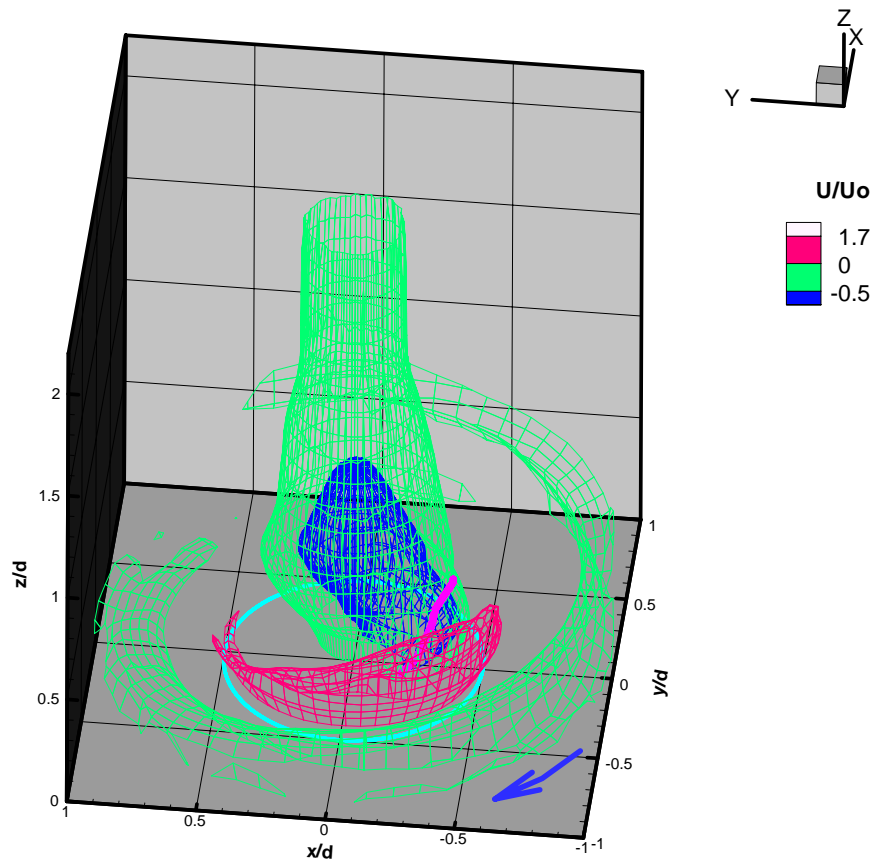


Fig. 5. Boundary of the reverse flow zone (green isosurface). The thick purple line indicates the PVC axis. The flowfield rotates in the direction shown by the blue arrow.

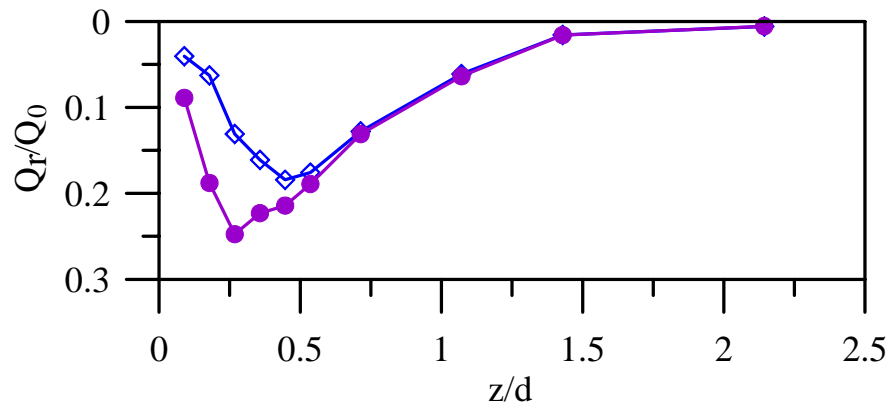


Fig. 6. Computed recirculating flow strength based on time-mean (squares) and phase-averaged (circles) data as a function of axial coordinate.

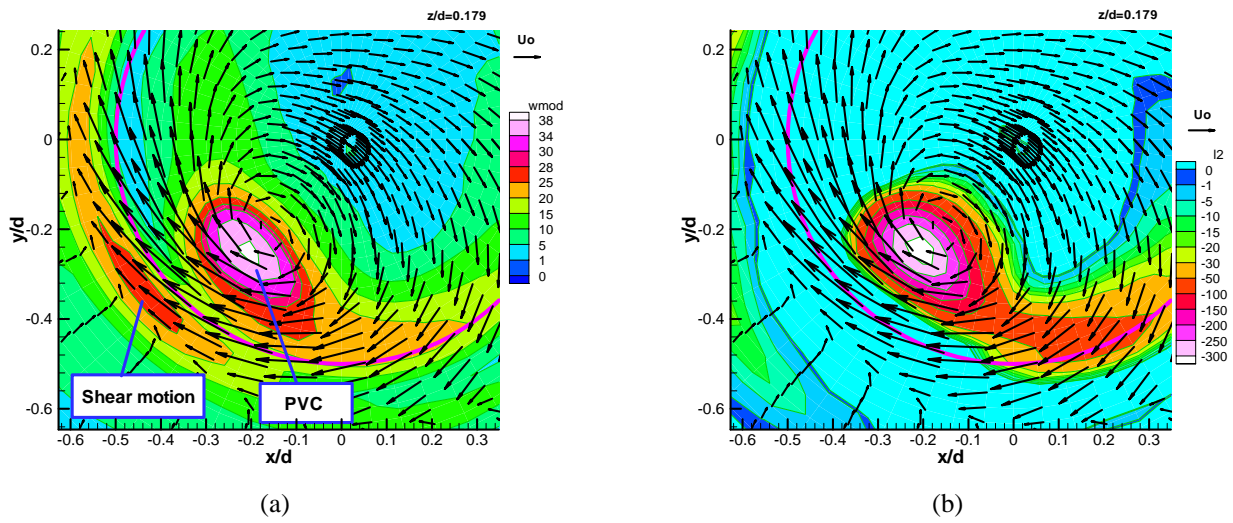


Fig. 7. Comparison of representation of a vortex core by absolute vorticity (a) and λ_2 (b) values.

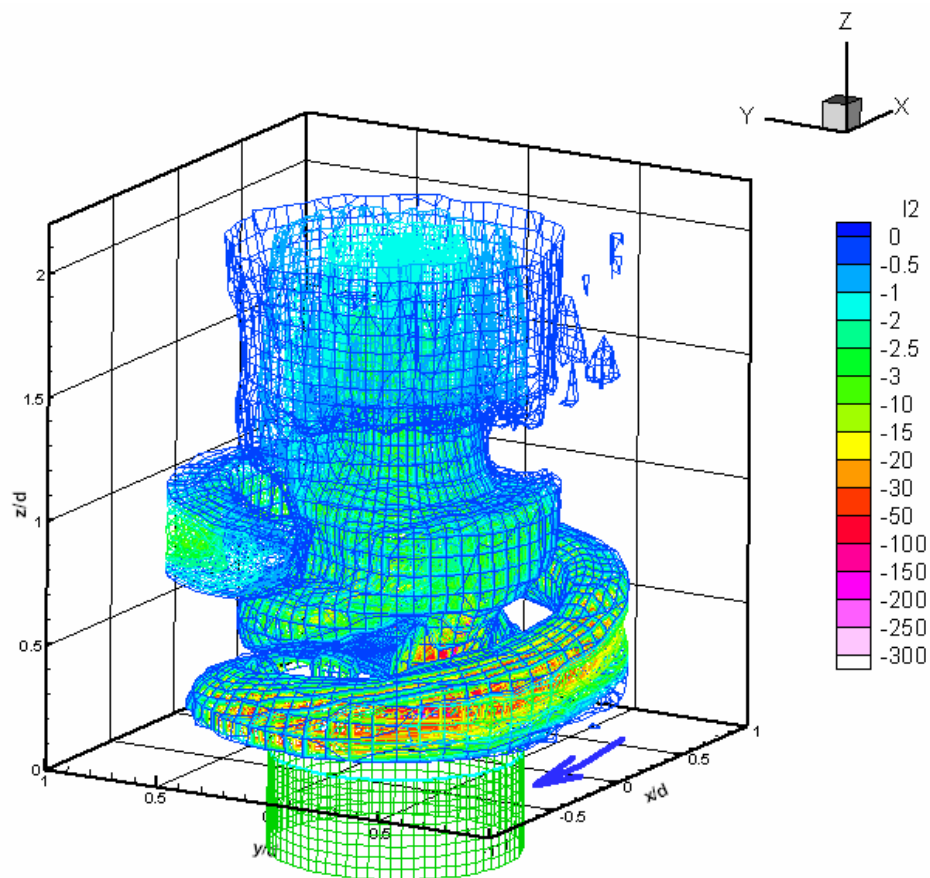


Fig. 8. Global flow structure visualised by means of λ_2 technique. Area with negative λ_2 enclosed in the blue contour surface corresponds to vortical motion. All the structures are rotating according to the blue arrow.

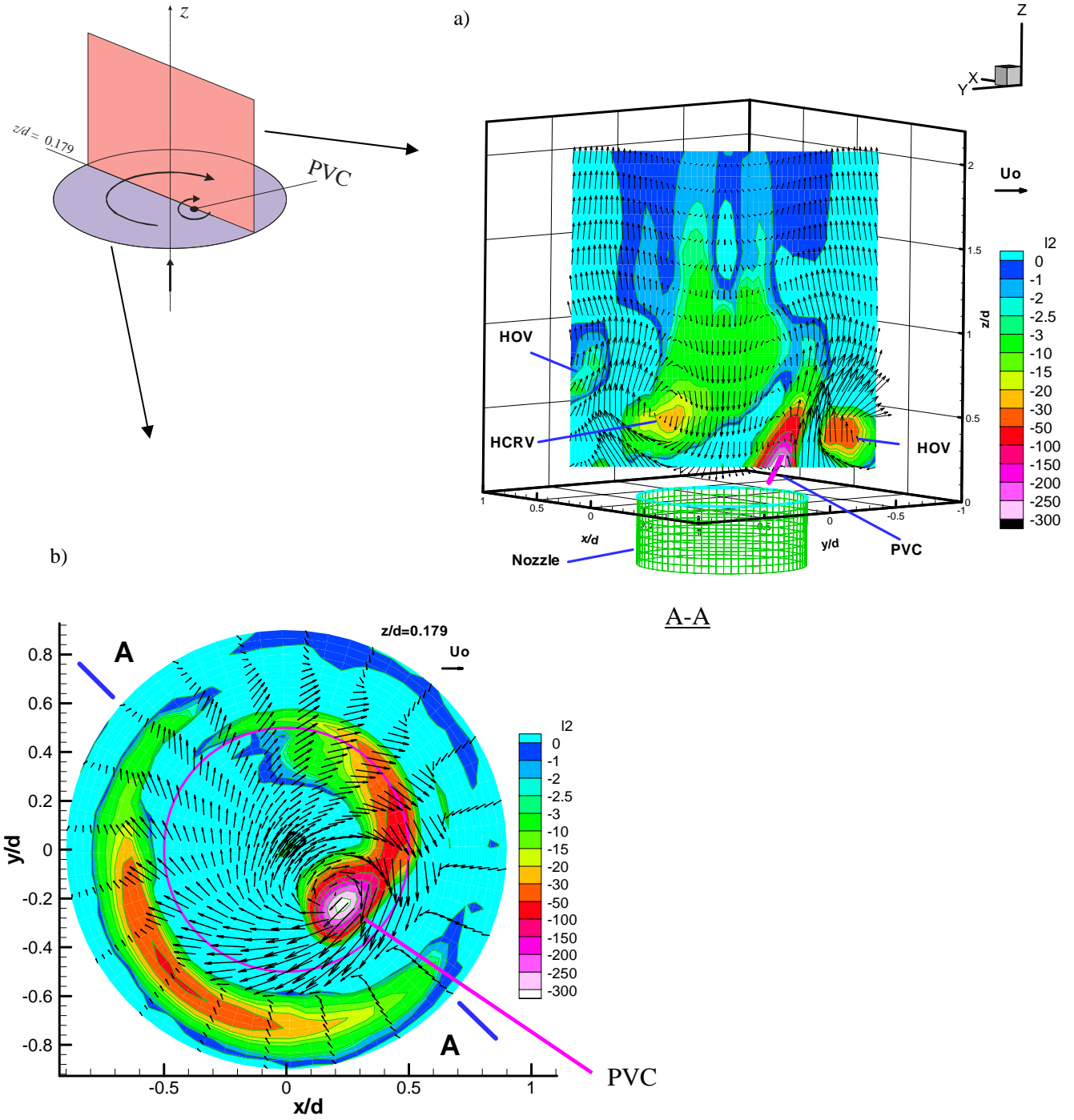
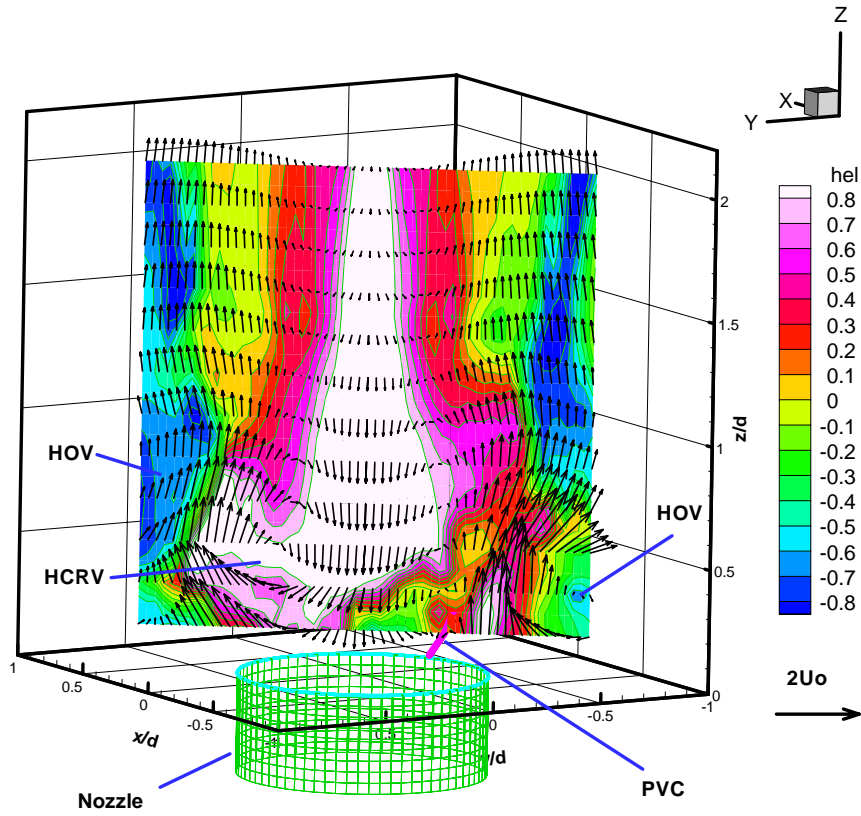


Fig. 9. Velocity maps superimposed on isoregions of λ_2 values:

- a) Vertical plane with radial-axial velocity components;
- b) Horizontal plane with radial-tangential velocity projections.



A-A

Fig. 10. Axial-radial velocity and normalised helicity isolines in a vertical cross-section (the same plane as in Fig. 9a).

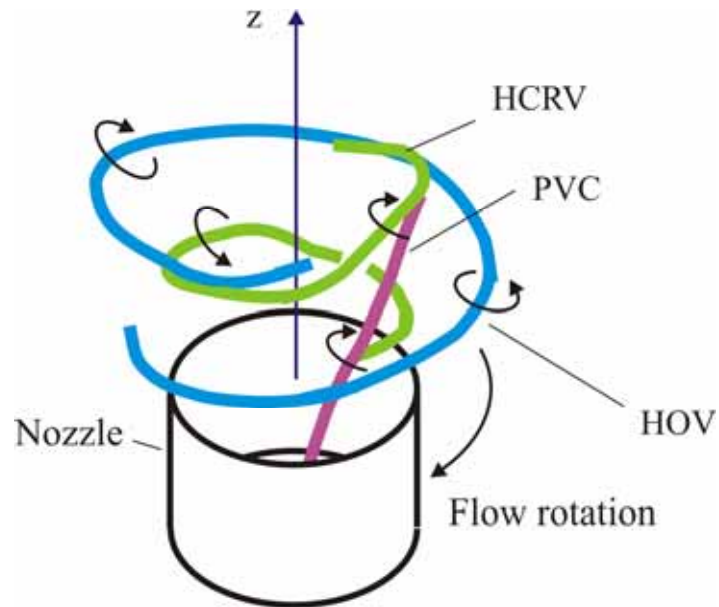


Fig. 11. Centre locations of the vortex structures identified based on λ_2 volume data.